Dynamic ^{11}C-PiB PET Shows Cerebrospinal Fluid Flow Alterations in Alzheimer Disease and Multiple Sclerosis

Julia J. Schubert[1], Mattia Veronese[1], Livia Marchitelli[1], Benedetta Bodini[2], Matteo Tonietto[2], Bruno Stankoff[2], David J. Brooks[3], Alessandra Bertoldo[4], Paul Edison[3], and Federico E. Turkheimer[1]

[1]Department of Neuroimaging, Institute of Psychiatry, Psychology and Neuroscience, King's College London, London, United Kingdom; [2]Sorbonne Universités, UPMC Paris 06, Institut du Cerveau et de la Moelle épinière, ICM, Hôpital de la Pitié Salpêtrière, Paris, France; [3]Imperial College London, London, United Kingdom; and [4]Department of Information Engineering, University of Padova, Padova, Italy

Cerebrospinal fluid (CSF) plays an important role in solute clearance and maintenance of brain homeostasis. ^{11}C-Pittsburgh compound B (PiB) PET was recently proposed as a tool for detection of CSF clearance alterations in Alzheimer disease. The current study investigates the magnitude of ^{11}C-PiB PET signal in the lateral ventricles of an independent group of Alzheimer and mild cognitive impairment subjects. We have also evaluated multiple sclerosis as a model of disease with CSF clearance alterations without amyloid-β tissue accumulation. **Methods:** A set of 11 Alzheimer and 12 mild cognitive impairment subjects and a set of 20 multiple sclerosis subjects with matched controls underwent MRI and dynamic ^{11}C-PiB PET. Lateral ventricle regions of interest were generated manually from MRI data. PET data were analyzed using cerebellum or a supervised reference region for the Alzheimer and multiple sclerosis data sets, respectively. The magnitude of ^{11}C-PiB signal in the lateral ventricles was calculated as area under the curve from 35 to 80 min and SUV ratio (SUVR) from 50 to 70 min. Compartmental modeling analysis was performed on a separate data set containing 11 Alzheimer and matched control subjects; this analysis included an arterial input function, to further understand the kinetics of the lateral ventricular ^{11}C-PiB signal. **Results:** ANOVA revealed significant group differences in lateral ventricular SUVR across the Alzheimer, mild cognitive impairment, and healthy control groups ($P = 0.004$). Pairwise comparisons revealed significantly lower lateral ventricular SUVR in Alzheimer subjects than in healthy controls ($P < 0.001$) or mild cognitive impairment subjects ($P = 0.029$). Lateral ventricular SUVR was significantly lower in multiple sclerosis subjects than in healthy controls ($P = 0.008$). Compartmental modeling analysis revealed significantly lower uptake rates of ^{11}C-PiB signal from blood ($P = 0.005$) and brain tissue ($P = 0.004$) to the lateral ventricles and significantly lower ^{11}C-PiB signal clearance out of the lateral ventricles ($P = 0.002$) in Alzheimer subjects than in healthy controls. **Conclusion:** These results indicate that dynamic ^{11}C-PiB PET can be used to observe pathologic changes in CSF dynamics. We have replicated previous work demonstrating CSF clearance deficits in Alzheimer disease associated with amyloid-β deposits and have extended the observations to include ventricular CSF clearance deficits in mild cognitive impairment and multiple sclerosis.

There has been great interest surrounding cerebrospinal fluid (CSF) dynamics since the existence of the glymphatic system was proposed in 2012 (*1–3*). The glymphatic system has been suggested as being largely responsible for the clearance of waste from the brain (*1,4*). The original description of the glymphatic system proposed that CSF penetrates the brain via paraarterial spaces; enters the brain parenchyma, where it combines with interstitial fluid and collects waste and other solutes; and returns to the subarachnoid space or clears through the vascular and lymphatic systems via paravenous spaces (Fig. 1A). This system is thought to be analogous to the body's peripheral lymphatic system with the additional involvement of glial cells (*1*). Although there is still debate over the mechanism underlying the glymphatic system (*2,3,5*), there is an overall agreement that a para- or perivascular clearance system of the brain exists and that it is closely linked to the production and flow of CSF.

CSF is produced predominantly by the choroid plexuses of the ventricular system. Interstitial fluid of surrounding brain tissues, excluding those of the circumventricular organs, exchanges quite freely with ventricular CSF because of the presence of gap junctions in the ependymal cell lining of the adult ventricular system that allow free diffusion of small molecules (*6*). CSF generally has a net positive flow through the ventricular system and out to the subarachnoid space that surrounds the brain and spinal cord (Fig. 1B). CSF is eventually cleared to the venous system through arachnoid villi, to the cervical lymphatics through the cribriform plate (*7,8*), or to the recently discovered meningeal lymphatics that line the dural sinuses (*9*). The transastrocytic water movements associated with CSF flow into and CSF/interstitial fluid flow out of the brain parenchyma are facilitated by aquaporin-4 water channels, which are localized along perivascular astrocytic end-feet that contribute to the blood–brain barrier (*1*).

The glymphatic system has been shown to contribute to clearance of amyloid-β (Aβ) (*1,10,11*), the main component of the amyloid plaques found in Alzheimer disease brain. Significant accumulation of Aβ has been observed after inhibition of glymphatic transport
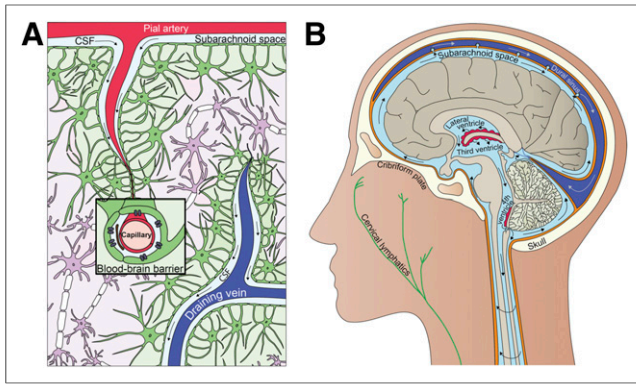
FIGURE 1. Interrelationship between clearance and fluid systems of brain. (A) Glymphatic system. (B) CSF system. (Illustrations by Julia J. Schubert.)

(10), and deletion of the aquaporin-4 gene suppresses clearance of soluble Aβ (1). Phase-contrast MRI has also shown significantly decreased CSF flow in multiple sclerosis patients compared with healthy controls (12,13), and associations have been observed between decreased CSF flow and conversion rate from clinically isolated syndrome to clinically defined multiple sclerosis and relapse rate in relapsing-remitting multiple sclerosis (12). Further, loss of perivascular aquaporin-4 localization has been observed in an experimental autoimmune encephalomyelitis mouse model of multiple sclerosis (14). These findings support a link between CSF flow alterations and neurologic diseases such as Alzheimer disease and multiple sclerosis.

Despite the current interest in CSF dynamics, noninvasive in vivo methods for measuring glymphatic function are limited, and most existing data have been collected using animal models (4,10,14). ^{11}C-Pittsburgh compound B (PiB) is a neutral lipophilic benzothiazole PET tracer and is used to image Aβ plaques in Alzheimer disease (15) and, more recently, to quantify in vivo myelin loss and regeneration in multiple sclerosis (16). ^{11}C-PiB PET has also recently been used to quantify CSF clearance in humans (8). Small-molecule radiotracers enter the CSF of the lateral ventricles directly from the blood through a thick epithelial cell layer of the choroid plexuses and from the brain parenchyma via diffusion through the ependymal cells that line the adult ventricular system (6). We aim to replicate previous results that showed decreased lateral ventricular ^{11}C-PiB signal magnitude in Alzheimer disease compared with controls (8) and to extend the method to mild cognitive impairment and multiple sclerosis patient groups. From previous research, each of these patient groups is expected to have altered CSF dynamics. However, because of differences in the pathogenesis of Alzheimer disease and multiple sclerosis, Aβ deposition is expected in only the Alzheimer disease and mild cognitive impairment groups. Inclusion of the multiple sclerosis group allows for further testing of our dynamic PET method for measuring CSF dynamics without the confounding factor of Aβ accumulation in brain tissue. We also aim to further understand the kinetics of the ^{11}C-PiB PET signal in the lateral ventricles by performing compartmental modeling analysis. Combined, these results will allow for appropriate interpretations about the lateral ventricular ^{11}C-PiB signal magnitude and how these measurements may relate to CSF-mediated clearance in healthy and diseased populations.

MATERIALS AND METHODS

Participants

To investigate differences in CSF clearance in Alzheimer disease and multiple sclerosis, analysis was performed on 2 data sets. One data set included 11 Alzheimer disease patients (6 women and 5 men; mean age, 66.5 ± 4.1 y), 12 mild cognitive impairment patients (4 women and 8 men; mean age, 68.6 ± 7.9 y), and 12 age- and sex-matched healthy controls (5 women and 7 men; mean age, 64.4 ± 6.6 y) who were recruited from Hammersmith Hospital NHS Trust, the National Hospital for Neurology and Neurosurgery, St. Margaret's Hospital, and Victoria Hospital. Recruitment of the healthy controls was aided by enrolment of spouses of the Alzheimer disease subjects. The Alzheimer disease and matched healthy control data have previously been reported alone (17) and with comparison to the mild cognitive impairment data (18). Clinically probable diagnoses of Alzheimer disease were assigned on the basis of the criteria of the National Institute of Neurologic and Communicative Diseases and Stroke/Alzheimer's Disease and Related Disorders Association and *Diagnostic and Statistical Manual of Mental Disorders,* fourth edition. All Alzheimer subjects also met the National Institute on Aging/Alzheimer's Association criteria. Alzheimer subjects aged 55 to 79 with a clinical diagnosis of Alzheimer disease before enrolment were included in the study. Patients and controls with a history of mental health issues, significant white matter microvascular disease on MRI, a contraindicative MRI result, a history of drug or alcohol abuse, or any other neurologic causes were excluded. Full details on inclusion and exclusion criteria for the Alzheimer subjects were reported in the original publication on this data set (17). Mild cognitive impairment subjects were chosen on the basis of exclusion criteria similar to those for the Alzheimer subjects and fulfilled Petersen's criteria for amnestic mild cognitive impairment (19). Six of the 12 mild cognitive impairment subjects were previously classified as amyloid-positive.

A second data set included 20 relapsing-remitting multiple sclerosis patients (13 women and 7 men; mean age, 32.3 ± 5.6 y) and 8 age- and sex- matched healthy controls (5 women and 3 men; mean age 31.6 ± 6.4 y). All patients were diagnosed with multiple sclerosis according to the revised McDonald criteria (20) and had at least one gadolinium-enhancing lesion when they entered the study. Additional information on inclusion and exclusion criteria can be found in the original report on this data set (16).

These studies were approved by the local ethics committees, and participants gave written informed consent before data collection.

Clinical Assessments

Alzheimer Disease/Mild Cognitive Impairment (AD/MCI) Data Set. Detailed neurologic assessments were performed for 9 Alzheimer subjects. These assessments included taking a patient history from a close relative, routine blood analysis, and electroencephalogram. The following neuropsychometric assessments were also performed: Mini-Mental State Examination (21), Warrington short recognition memory tests for words and faces, Alzheimer Disease Assessment Scale Word List Learning test and 30-min delayed recall (22), immediate and delayed recall of modified complex figure (23), Digit Span forwards (24), Trail Making Part A (25), clock drawing (26), copy of modified complex figure (23), 30-item Boston Naming Test (27), letter fluency (F-A-S test) (28), and category fluency (animals, birds, and dogs). All mild cognitive impairment subjects also underwent a comprehensive assessment that included neurologic examination, neuropsychologic testing, and MRI.

Multiple Sclerosis Data Set. The Expanded Disability Status Scale (29) and Multiple Sclerosis Severity Scale (30) were used to rate 19 multiple sclerosis subjects at the time of enrolment.

Demographic data from the Alzheimer, mild cognitive impairment, multiple sclerosis, and matched control groups are included in Supplemental Table 1 (supplemental materials are available at http://jnm.snmjournals.org).

PET and MRI Data Acquisition

AD/MCI Data Set. All subjects had 90-min ^{11}C-PiB PET on a Siemens ECAT EXACT HR+ scanner with 3-dimensional acquisition and an axial field of view of 15.5 cm. All subjects were given an intravenous bolus injection of ^{11}C-PiB (mean, 365 ± 24 MBq) at the start of each scan. Image reconstruction and data processing, including scatter correction, were performed using standard Siemens software. All subjects also had MRI, which was performed with a 1.5-T GE Healthcare scanner. The T1-weighted structural MRI data were used for region-of-interest (ROI) segmentation. Additional information on the PET and MRI protocols can be found in the original reports on these data (17,18).

Multiple Sclerosis Data Set. A High-Resolution Research Tomograph (CPS Innovations) was used to perform a 90-min ^{11}C-PiB PET scan on all subjects. All subjects were given an intravenous bolus injection of ^{11}C-PiB (mean, 358 ± 34 MBq) at the start of each scan. An intraslice spatial resolution of about 2.5 mm full width at half maximum was achieved, with 25 cm axial and 31.2 cm transaxial fields of view. A Poisson ordered-subset expectation maximization algorithm with 10 iterations was used for image reconstruction. To assist in reducing the effects of partial volume in the multiple sclerosis data set (31), the reconstructed images were smoothed with a filter implementing point-spread function. All subjects also underwent MR scanning on a 3-T Siemens Trio 32-channel Total Imaging Matrix system. T1-weighted structural MRI data collected before gadolinium injection were used for ROI segmentation in this work. The PET image acquisition, reconstruction, and quantification techniques have been previously described (32). Additional information on the PET and MRI protocols can be found in the original report on this data set (16).

Data Analysis

AD/MCI Data Set. Preprocessing of the PET and MRI data from the AD/MCI data set was performed and time–activity curves were generated using MIAKAT software (version 4.2.6) (33). MIAKAT is implemented in MATLAB (version R2015b; The MathWorks, Inc.), and the preprocessing pipeline uses tools from SPM12 and FSL (version 5.0.9) analysis toolboxes (34) to perform brain extraction, tissue segmentation, rigid and nonlinear registration to the Montreal Neurological Institute template (35), ROI definition, and motion correction. An additional gray matter ROI was defined that excluded the cerebellum reference region. The data sets of one Alzheimer and one mild cognitive impairment subject did not pass quality control because of misregistration artifacts and were excluded from the AD/MCI analysis.

Multiple Sclerosis Data Set. Motion correction of the multiple sclerosis data set was performed by realigning each PET frame to a common reference space, as has been previously described (36). T1-weighted MR images were registered to the ^{11}C-PiB PET images. A priori designated ROIs were used for a supervised reference region and a gray matter ROI used in the multiple sclerosis analysis. The gray matter ROI excluded reference and cerebellar gray matter for comparison with the Alzheimer data set. Time–activity curve extraction for the multiple sclerosis data set was performed using in-house MATLAB (version R2017a) scripts.

For both data sets, manual lateral ventricle ROIs were generated for all subjects using the subject T1-weighted structural MRI data and the ITK-SNAP (www.itksnap.org) snake tool (37), following previously described guidelines for lateral ventricle extraction (38). The lateral ventricle ROIs were then eroded by 2 voxels (5.2 mm) using the erode

function given by the FSL "fslmaths" utility package (version 5.0.9) (34) to reduce partial-volume effects of the surrounding tissues. An example lateral ventricle ROI is shown in Supplemental Figure 1.

SUV ratios (SUVRs) from 50 to 70 min were calculated for the gray matter and lateral ventricle ROIs for each subject from both data sets using cerebellum or a supervised reference region for the AD/MCI and multiple sclerosis data sets, respectively. For consistency with a previous study (8), the area under the curve (AUC) from 35 to 80 min ($AUC_{35–80}$) was also calculated for the lateral ventricle ROI for a subset of the AD/MCI data set. $AUC_{35–80}$ was also calculated for the lateral ventricle ROI for all subjects in the multiple sclerosis data set.

Compartmental Modeling Analysis

Participants. A data set that included 11 Alzheimer disease subjects and 11 age- and sex-matched healthy controls was included for sole use in compartmental modeling analysis. These data have been previously reported (39). All Alzheimer subjects in this data set met the National Institute of Neurologic and Communicative Diseases and Stroke/Alzheimer's Disease and Related Disorders Association criteria for probable Alzheimer disease and had Mini-Mental State Examination scores greater than 16 at study inclusion. Healthy controls were recruited by advertisement or during participation in a separate long-term follow-up study in the clinic. This study was approved by the local ethics committee, and all participants gave written informed consent before data collection.

PET Data Acquisition. All subjects underwent 90-min ^{11}C-PiB PET with online arterial sampling. PET data were collected on an ECAT EXACT H+ scanner (Siemens/CTI). Metabolite-corrected arterial input functions were determined using the measured percentage of radioactive parent compound in plasma. Further details about the PET protocol can be found in the original report on this data set (39).

Compartmental Model. The final model used to describe ^{11}C-PiB PET kinetics in the lateral ventricles is shown in Figure 2. This model includes 2 compartments to account for the signal from both bound and unbound ventricle pools and 2 input functions. One input function corresponds to the whole-brain gray matter, which describes the tracer transport from the brain tissue into the lateral ventricles, and one input function corresponds to the parent plasma arterial input function, which describes the tracer transport from the blood into the lateral ventricles. This model was determined on the basis of the known biologic restraints of the CSF system (6).

Data Analysis. Compartmental modeling analysis was performed with SAAM II software (40). The lateral ventricle ROI used for time–activity curve extraction was defined using a registered Montreal
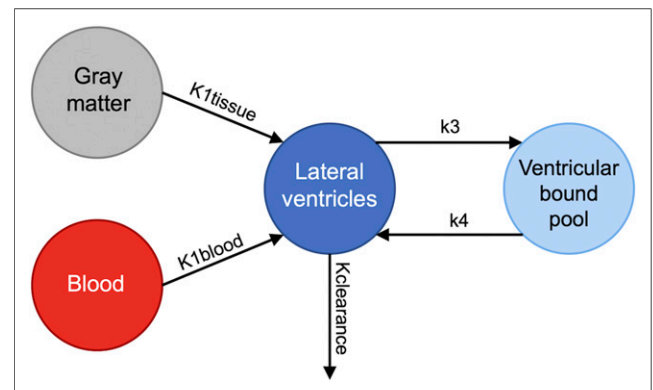

FIGURE 2. Kinetic model used in compartmental modeling analysis. $K_{clearance}$ includes total clearance from lateral ventricles to blood, tissue, and rest of ventricular system.

Neurological Institute template and the ITK-SNAP snake tool (37) with additional manual drawing when necessary. This data set was used because it included an arterial input function necessary for accurate signal measurements from the blood, which is required for compartmental modeling analysis. Visual inspection of the Montreal Neurological Institute template–generated lateral ventricle ROIs overlaid on individual subjects' PET images showed good overlap with the areas known to be lateral ventricle CSF in all cases. The rate constants $K_{clearance}$, $K_{1tissue}$, K_{1blood}, k_3, and k_4 represent the rate of ^{11}C-PiB signal between tissues in the system. $K_{clearance}$ takes into account the clearance of signal from the lateral ventricles to blood, surrounding tissues, and the rest of the ventricular system because it is not possible to differentiate between these clearance pathways. The SAAM II software was used to iteratively fit the time–activity curve data to the model, and final values of the rate constants were recorded for each subject.

Statistical Analyses

All statistical analyses were performed in SPSS (version 24.0). The Shapiro–Wilk W test was used to test for normality of the data. ANOVA was used to investigate group differences in lateral ventricle and gray matter ^{11}C-PiB signal in the AD/MCI data set. Paired differences in lateral ventricle ^{11}C-PiB SUVRs between groups in the AD/MCI and multiple sclerosis data sets were investigated using independent-samples t tests. Paired differences in lateral ventricle ^{11}C-PiB AUC_{35-80} between groups were investigated using independent-samples t tests for the AD/MCI data set and the Mann–Whitney U test for the multiple sclerosis data set. Paired differences in gray matter ^{11}C-PiB SUVRs between groups were investigated using the Mann–Whitney U test for the AD/MCI data set and an independent-samples t test for the multiple sclerosis data set. Spearman correlation was used to investigate the relationship between gray matter and

lateral ventricular ^{11}C-PiB signal as well as between clinical scores and lateral ventricular ^{11}C-PiB signal in Alzheimer disease and multiple sclerosis patient groups. Group differences in $K_{clearance}$, k_3, and k_4 were investigated using independent-samples t tests. Group differences in $K_{1tissue}$ and K_{1blood} were investigated using the Mann–Whitney U test. Brain size and ventricle size were tested as possible covariates.

RESULTS

Lateral Ventricular ^{11}C-PiB Signal Magnitude in Relation to Diagnosis

ANOVA revealed significant group differences in lateral ventricle SUVRs across the Alzheimer disease, mild cognitive impairment, and healthy control groups ($F_{2,30} = 6.86$, $P = 0.004$), which remained significant when corrected for ventricle size ($F_{2,29} = 3.34$, $P = 0.050$). Brain size was not found to be a significant covariate in the AD/MCI data set. Additional pairwise comparisons revealed a significantly lower magnitude of lateral ventricular ^{11}C-PiB, as measured by SUVR, in Alzheimer disease subjects (mean, 0.37; SD, 0.09) than in healthy controls (mean, 0.57; SD, 0.15) ($t_{18} = 4.08$, $P < 0.001$) or mild cognitive impairment subjects (mean, 0.49, SD, 0.14) ($t_{19} = 2.36$, $P = 0.029$). No significant difference in lateral ventricle SUVR was observed between mild cognitive impairment subjects and healthy controls ($t_{21} = 1.37$, $P = 0.185$) (Fig. 3A). Lateral ventricle AUC_{35-80} was significantly lower in Alzheimer disease subjects (mean, 0.47; SD, 0.13) than in healthy controls (mean, 0.72; SD, 0.20) ($t_{18} = 3.32$, $P = 0.004$) or mild cognitive impairment subjects (mean, 0.65; SD, 0.18) ($t_{17} = 2.47$, $P = 0.024$). ANOVA also revealed significant group differences in lateral ventricle AUC_{35-80} across the Alzheimer disease, mild cognitive impairment, and healthy control groups ($F_{2,26} = 5.53$, $P = 0.010$) (Fig. 3B).

Lateral ventricle ^{11}C-PiB SUVRs were significantly lower in multiple sclerosis (mean, 0.77; SD, 0.19) than in healthy controls (mean, 1.01; SD, 0.21) ($t_{26} = 2.87$, $P = 0.008$), which remained significant when corrected for ventricle size ($F_{1,25} = 4.35$, $P = 0.047$) (Fig. 3C). Brain size was not found to be a significant covariate in the multiple sclerosis data set. There were no other significant differences in AUC_{35-80} measurements between groups.

Correlations with Tissue ^{11}C-PiB

We observed significant negative correlations in ^{11}C-PiB SUVRs between gray matter and lateral ventricle ROIs in mild cognitive impairment subjects ($r = -0.664$, $P = 0.026$) and AD/MCI-matched control subjects ($r = -0.909$, $P < 0.001$), which was not observed in Alzheimer disease subjects ($r = -0.479$, $P = 0.162$) (Fig. 4A). No significant correlations were observed between gray matter ^{11}C-PiB SUVRs and lateral ventricle AUC_{35-80} in Alzheimer disease subjects ($r = -0.182$, $P = 0.614$), mild cognitive impairment subjects ($r = -0.150$, $P = 0.700$), or AD/MCI-matched control subjects ($r = -0.115$, $P = 0.751$) (Fig. 4B).
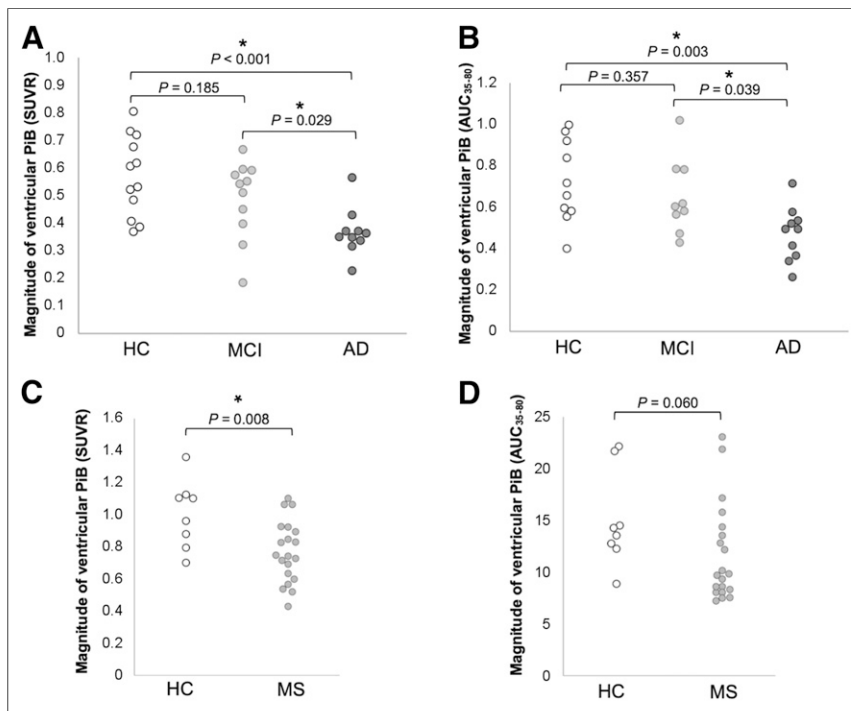

FIGURE 3. Group differences in lateral ventricle ^{11}C-PiB measurements. (A) Lateral ventricle ^{11}C-PiB SUVR in healthy controls (HC), mild cognitive impairment (MCI), and Alzheimer disease (AD). (B) Lateral ventricle ^{11}C-PiB AUC_{35-80} in HC, MCI, and AD. (C) Lateral ventricle ^{11}C-PiB SUVR in HC and multiple sclerosis (MS). (D) Lateral ventricle ^{11}C-PiB AUC_{35-80} in HC and MS. Significant differences ($P < 0.05$) are indicated by an asterisk.
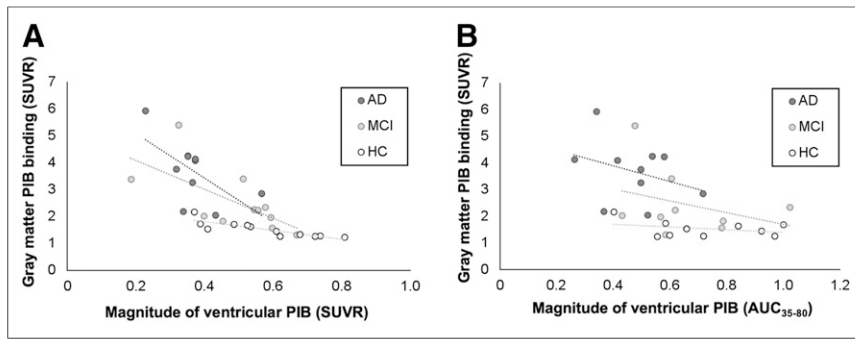
FIGURE 4. Correlations between gray matter ^{11}C-PiB SUVR and lateral ventricle ^{11}C-PiB SUVR (A) and AUC$_{35-80}$ (B) in Alzheimer disease (AD), mild cognitive impairment (MCI), and healthy controls (HC). In A, $r = -0.479$ and $P = 0.162$ for AD, $r = -0.664$ and $P = 0.026$ for MCI, and $r = -0.909$ and $P < 0.001$ for HC. In B, $r = -0.182$ and $P = 0.614$ for AD, $r = -0.150$ and $P = 0.700$ for MCI, and $r = -0.115$ and $P = 0.751$ for HC.

We did not observe any significant ^{11}C-PiB signal correlations between gray matter and lateral ventricle regions in the multiple sclerosis subjects (SUVR: $r = 0.045$, $P = 0.850$; AUC$_{35-80}$: $r = -0.170$, $P = 0.945$) or multiple sclerosis–matched control subjects (SUVR: $r = 0.333$, $P = 0.420$; AUC$_{35-80}$: $r = -0.238$, $P = 0.570$).

Gray Matter ^{11}C-PiB Signal Magnitude in Relation to Diagnosis

ANOVA revealed significant group differences in gray matter SUVRs across Alzheimer disease, mild cognitive impairment, and healthy control groups ($F_{2,30} = 14.53$, $P < 0.001$). Gray matter ^{11}C-PiB signal, as measured by SUVR, was significantly higher in Alzheimer disease subjects (mean, 3.68; SD, 1.14) than in healthy controls (mean, 1.53; SD, 0.28) ($U = 119.0$, $P < 0.001$) or mild cognitive impairment subjects (mean, 2.52; SD, 1.15) ($U = 87.0$, $P = 0.024$) and was significantly higher in mild cognitive impairment subjects than in healthy controls ($U = 116.0$, $P = 0.002$) (Fig. 5A). Gray matter ^{11}C-PiB SUVRs were not significantly different between multiple sclerosis subjects and healthy controls ($t_{26} = 1.32$, $P = 0.198$) (Fig. 5B).

Correlations with Disease Severity Measures

AD/MCI Data Set. We did not observe any significant correlations between Mini-Mental State Examination and lateral ventricle SUVRs in the Alzheimer disease group ($r = -0.042$, $P = 0.914$). No other
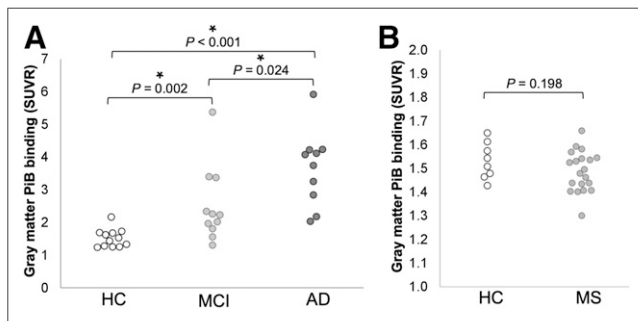

FIGURE 5. Group differences in gray matter ^{11}C-PiB SUVRs. (A) Gray matter ^{11}C-PiB SUVR in healthy controls (HC), mild cognitive impairment (MCI), and Alzheimer disease (AD). (B) Gray matter ^{11}C-PiB SUVR in HC and multiple sclerosis (MS). Significant differences ($P < 0.05$) are indicated by an asterisk.

significant correlations were observed between disease severity measures and lateral ventricle ^{11}C-PiB measures in the Alzheimer disease group.

Multiple Sclerosis Data Set. We did not observe any significant correlations between Multiple Sclerosis Severity Scale ($r = 0.075$, $P = 0.762$), Expanded Disability Status Scale ($r = -0.003$, $P = 0.991$), or disease duration ($r = -0.144$, $P = 0.555$) and lateral ventricle SUVRs. We observed significant correlations between lesion load, as defined by the volume of white matter lesions, and lateral ventricle SUVRs ($r = -0.493$, $P = 0.032$) and AUC$_{35-80}$ ($r = -0.595$, $P = 0.007$) (Fig. 6). We did not observe any other statistically significant correlations between disease severity measures and lateral ventricle ^{11}C-PiB signal measures in the multiple sclerosis group.

Compartmental Modeling Analysis

The final compartmental model used in our analysis reliably fit the lateral ventricle time–activity curve data. Example fits of the lateral ventricle time–activity curve data from one healthy control and one Alzheimer disease subject using the final compartmental model are shown in Supplemental Figure 2.

Results from compartmental modeling analysis revealed significant group differences in rates of ^{11}C-PiB signal exchange across tissues between Alzheimer disease and healthy control subjects. The rate of signal from blood to the lateral ventricles ($K_{1\text{blood}}$) ($U = 13.0$, $P = 0.005$), from tissue to the lateral ventricles ($K_{1\text{tissue}}$) ($U = 12.0$, $P = 0.004$), and from the lateral ventricles to blood, tissue, and the rest of the ventricular system ($K_{\text{clearance}}$) ($t_{18} = 3.70$, $P = 0.002$) was significantly lower in Alzheimer disease subjects than in healthy controls (Fig. 7). We did not observe any other significant differences between groups.

Simplified compartmental models, including one without specific binding in the lateral ventricles and one without a brain tissue input function, were also compared with the final compartmental model used in our analysis. The final model used was superior to simplified models, as determined by comparison of Akaike information criterion scores.

DISCUSSION

Our observation of decreased ^{11}C-PiB signal in the lateral ventricle ROIs in Alzheimer disease and multiple sclerosis patient groups compared with healthy controls indicates that dynamic PET measures can be used to observe pathologic changes in CSF dynamics. We have successfully replicated a previous study that showed decreased lateral ventricle ^{11}C-PiB signal in Alzheimer disease compared with healthy controls (8). Here, we have also shown that lateral ventricle ^{11}C-PiB is significantly lower in multiple sclerosis subjects than in healthy controls and that mild cognitive impairment subjects have ^{11}C-PiB measures intermediate between those of healthy controls and Alzheimer disease subjects. We replicated previous work showing an inverse correlation between gray matter and lateral ventricle ^{11}C-PiB binding in Alzheimer disease, and we show that this correlation is present in mild cognitive impairment subjects and AD/MCI-matched healthy controls. Our compartmental modeling analysis reveals that the reduced lateral
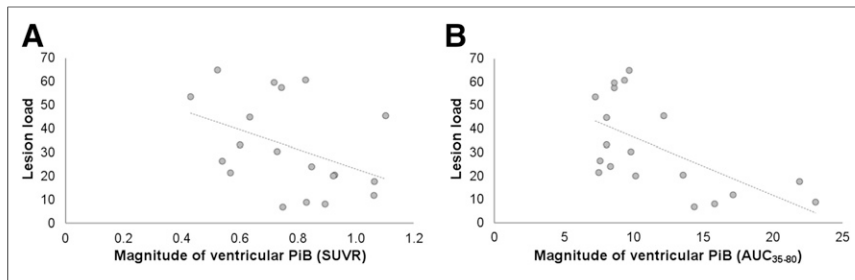
FIGURE 6. Lateral ventricle ^{11}C-PiB measures and lesion load correlations. (A) Correlation between lesion load and lateral ventricle SUVRs in multiple sclerosis (MS) ($r = -0.493$, $P = 0.032$). (B) Correlation between lesion load and lateral ventricle AUC_{35-80} in MS ($r = -0.595$, $P = 0.007$). Lesion load is defined as volume of white matter lesions.

ventricle signal is likely due to decreased tracer entering the lateral ventricles through the blood and through the brain tissue in Alzheimer disease compared with healthy controls. This analysis also shows that tracer is cleared from the lateral ventricles to the surrounding tissues and the ventricular system at a lower rate in Alzheimer disease subjects than in healthy controls. Our results also indicate that the reduction of tracer entering and leaving the lateral ventricles in patient groups is independent of Aβ deposition, as indicated by the lateral ventricle PET results from the multiple sclerosis data set, which is not expected to have significant Aβ accumulation in tissue. This is further supported by our observation of no significant difference in ^{11}C-PiB signal in gray matter between multiple sclerosis patients and controls, in contrast to the higher ^{11}C-PiB signal observed in Alzheimer disease gray matter. Altogether, these results suggest that CSF-mediated tissue clearance is reduced in Alzheimer disease and multiple sclerosis subjects compared with healthy controls.

Increasing age is considered a major risk factor in the development of Alzheimer disease (*41*), and Aβ deposition has been associated with increasing age in cognitively normal individuals without Alzheimer disease (*42*). The observed inverse relationship between gray matter and lateral ventricle ^{11}C-PiB signal in mild cognitive impairment and control groups could indicate that tissue CSF clearance alterations are associated with Aβ deposition before Alzheimer disease onset. Under the pathogenic conditions of Alzheimer disease, there are likely additional factors related to the disease that contribute to further Aβ deposition (*43*), which weakens the linear relationship between CSF clearance and tissue Aβ deposition. This could explain why we did not observe the inverse relationship between CSF clearance and Aβ deposition measures in the Alzheimer disease group. However, because of the greater

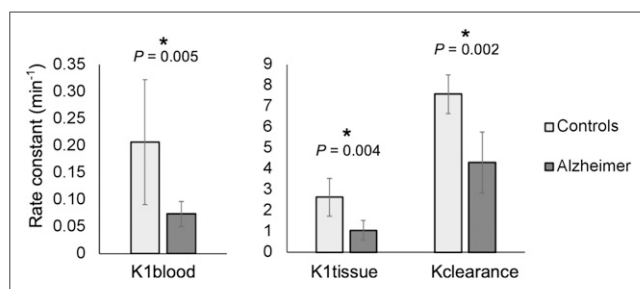**FIGURE 7.** Results from compartmental modeling analysis: healthy controls and Alzheimer group differences in K_{1blood}, $K_{1tissue}$, and $K_{clearance}$ rates. Error bars represent 95% confidence intervals. Significant differences ($P < 0.05$) are indicated by an asterisk.

heterogeneity in tissue ^{11}C-PiB measures in the Alzheimer disease and mild cognitive impairment groups, we may be lacking the statistical power necessary to measure the correlations in these groups. Additional mechanistic analysis with a larger cohort would be helpful in drawing further conclusions about these results. We did not observe an inverse relationship between gray matter and lateral ventricle ^{11}C-PiB in multiple sclerosis or multiple sclerosis–matched controls, likely because of the younger age of the cohort or a different mechanism of the disease that does not typically involve Aβ accumulation. The positive correlation between lesion load and ^{11}C-PiB signal in the multiple sclerosis group may indicate that CSF clearance alterations play a role in ongoing disease activity in multiple sclerosis.

Previous literature has reported decreased Aβ clearance from the brain in Alzheimer disease (*44*), but it has been unclear whether this decrease is due to reduced membrane transport from tissue to the CSF or from reduced clearance of the CSF through the CSF system. Compartmental modeling analysis allows us to make further inferences regarding where changes in Aβ clearance are occurring and which tissue types and systems may be responsible. We see that the change in Aβ clearance in Alzheimer disease is likely due to both reduced clearance of Aβ from the tissue to the CSF and reduced clearance of CSF through the CSF system. It remains unclear whether alterations to one of these processes precede alterations to the other. Additional compartmental modeling analyses using data from other patient groups (including multiple sclerosis, clinically isolated syndrome, mild cognitive impairment, and subjects with first signs of Aβ accumulation) would be useful for drawing further conclusions about our results.

The explanation as to why CSF-mediated clearance is reduced in neurologic diseases such as Alzheimer disease and multiple sclerosis is not entirely clear. Previous research has shown that sleep is important for glymphatic system function and consequently the clearance of waste from the brain (*45*). Sleep disorders are common in both Alzheimer disease (*46*) and multiple sclerosis (*47*) and may play a part in the onset of disease and could contribute to the ongoing disease processes. Additionally, synaptic activity has been linked to increased levels of Aβ in interstitial fluid (*48*), and voluntary exercise has been shown to increase clearance of Aβ by the glymphatic system in aged mice (*49*). These findings suggest that physical activity also plays a role in brain clearance. Further, physical activity has been shown to be effective in preventing the onset of and improving outcomes in Alzheimer disease (*50*) and may also contribute to improved sleep quality in health (*51*) and neurologic disease (*52,53*). Previous work has shown reduced sleep quality before the onset of cognitive decline in Alzheimer disease (*54*). However, additional research is still required to investigate whether inactivity or sleep disturbances precede the onset of disease, which may help further explain the initial pathophysiology that leads to disease onset.

Additional explanations for alterations in CSF-mediated clearance in aged and Alzheimer disease brain could be attributed to changes in the barriers that exist between brain tissue, blood, and CSF. Age is associated with cellular atrophy and decreased cell height of the choroid plexuses, which is exacerbated in Alzheimer

disease (55). The production of CSF and removal of solutes from the CSF by the choroid plexuses are active processes (56), and the cells become less energy-efficient with age (57). Age-related changes to the cells of the choroid plexuses contribute to decreased clearance of solutes to the blood as well as decreased CSF production, resulting in slower CSF turnover and reduced CSF-mediated brain clearance. The ependymal cells that line the ventricular system also flatten with age and exhibit greater dispersion in cilia expression (58), which normally contributes to flow of CSF and communication across the ependymal layer (59). These age-related changes to the ependymal layer likely contribute to decreased CSF-mediated brain clearance.

A previous MRI study revealed irregularities in the ependymal layer in early multiple sclerosis that have been attributed to ependymal perivenular inflammation (60). Inflammation of the choroid plexuses in multiple sclerosis has also been observed (61). Under healthy conditions, immune surveillance of the brain is partly accomplished by lymphocyte entry to the CSF through the choroid plexuses (62). Initial entry of reactive lymphocytes through the choroid plexuses was observed before lymphocyte infiltration into brain tissue across the blood–brain barrier in a mouse model of multiple sclerosis (63), which provides support for the involvement of the choroid plexuses in multiple sclerosis disease onset. The alterations to the ventricular barriers in multiple sclerosis could be both a cause and a consequence of impaired CSF-mediated clearance mechanisms, and further work is required to better understand the relationship and chronology of these changes.

Additional work will be done to investigate whether our ^{11}C-PiB PET results are specific to Alzheimer disease and multiple sclerosis or whether CSF clearance is also altered in other neurologic disorders. Further, we will look into use of other dynamic PET tracers and integration of quantitative MRI and CSF biomarker measures for assessing and understanding CSF-mediated clearance. It will also be helpful to explore how manipulation of known glymphatic system modulators affects the dynamic PET measures, which will allow for more informed interpretations of the results given from these PET measures in the future.

Our study had some limitations. Although we still observed statistically significant differences between groups when including ventricle size as a covariate in the AD/MCI and multiple sclerosis data sets, this may not be an appropriate way to correct for ventricle size. Larger ventricle size is an inherent feature of Alzheimer disease, and we observe significant group differences in ventricle size across the Alzheimer disease, mild cognitive impairment, and healthy control groups in the current analysis ($P = 0.041$), most notably between Alzheimer disease and healthy controls ($P = 0.001$). Simply adding ventricle size as a covariate may, therefore, be statistically inappropriate for use in our model because we are likely removing variance between groups that exists due to disease. Additional work should be performed to investigate more appropriate ways to accommodate for differences in ventricle size in the future.

We are restricted in our compartmental modeling analysis by the absence of structural image data in the form of MRI or CT for the selected Alzheimer disease data set. We produced all lateral ventricle ROIs for the compartmental modeling using a registered Montreal Neurological Institute template for each subject. Registered Montreal Neurological Institute templates are not as reliable for defining brain structures as MRI or CT images, and our lateral ventricle ROIs for compartmental modeling analysis are therefore prone to error. Our selection of ^{11}C-PiB PET data sets was restricted to those that included an arterial input function that is required for compartmental modeling analysis. However, the invasive nature of continuous arterial blood sampling discourages use of arterial input functions in human studies. Ideally, future PET studies will be designed to include arterial blood sampling during PET data collection for use in compartmental modeling analysis.

Our compartmental model has several limitations. The model uses time–activity curve data from all gray matter for the tissue pool that exchanges with the lateral ventricles. However, we expect direct exchange only between the deep gray matter structures and the lateral ventricular CSF because of their proximity to each other. However, these regions of direct exchange are difficult to define, and signal from whole gray matter is expected to behave similarly to the signal in the deep gray matter structures alone. Therefore, signal from whole gray matter was used as a representative measure for the gray matter that exchanges with the lateral ventricle CSF. We also tested a model using signal from cerebellar gray matter as a region that is not expected to have specific binding in Alzheimer disease (Supplemental Fig. 3) to confirm that the differences in rate constants between groups are not driven by differences in gray matter signal due to specific binding to Aβ. A model that entirely excluded input from the gray matter tissue to the lateral ventricles (Supplemental Fig. 4) resulted in poorer fits of the lateral ventricle time–activity curve data, indicating that this simplified model is inferior in its ability to represent the system. Finally, it is unclear what the specific binding in the lateral ventricles represents in our model. This bound pool may be accounted for by tracer binding to the ventricle walls or choroid plexuses or, less likely, to compounds within the CSF. We found that a model that excluded the ventricular bound pool (Supplemental Fig. 5) did not reliably fit the lateral ventricle time–activity curve data, indicating that this simplified model does not accurately represent the system.

CONCLUSION

The results from this work confirm that dynamic ^{11}C-PiB PET can be used to assess CSF dynamics in health and neurologic disease. In this work, we present a successful replication of previous results that showed CSF-mediated clearance deficits in Alzheimer disease associated with amyloid-β deposits (8). We also extend the observation to include CSF-mediated clearance deficits in mild cognitive impairment and multiple sclerosis. Our results provide further support for a promising method for assessing brain clearance in neurologic disease. We hope that this and future work in this area will improve the understanding of the pathogenesis of neurologic diseases such as Alzheimer disease and multiple sclerosis.

DISCLOSURE

ACKNOWLEDGMENTS

KEY POINTS

QUESTION: Do cerebrospinal fluid flow alterations exist in multiple sclerosis and Alzheimer disease?

PERTINENT FINDINGS: This case-control study further supports the use of dynamic ^{11}C-PiB PET to assess cerebrospinal fluid dynamics in health and disease. We observed significantly lower lateral ventricle ^{11}C-PiB signal in multiple sclerosis and Alzheimer disease patient groups than in healthy controls, indicating that alterations to cerebrospinal fluid–mediated brain clearance may be present in these diseases.

IMPLICATIONS FOR PATIENT CARE: These findings improve our understanding of pathologic mechanisms of multiple sclerosis and Alzheimer disease and support the use of our imaging method as a biomarker for investigating cerebrospinal fluid–mediated brain clearance.

REFERENCES

1. Iliff JJ, Wang M, Liao Y, et al. A paravascular pathway facilitates CSF flow through the brain parenchyma and the clearance of interstitial solutes, including amyloid β. *Sci Transl Med.* 2012;4:147ra111.
2. Bakker ENTP, Bacskai BJ, Arbel-Ornath M, et al. Lymphatic clearance of the brain: perivascular, paravascular and significance for neurodegenerative diseases. *Cell Mol Neurobiol.* 2016;36:181–194.
3. Bacyinski A, Xu M, Wang W, Hu J. The paravascular pathway for brain waste clearance: current understanding, significance and controversy. *Front Neuroanat.* 2017;11:101.
4. Iliff JJ, Wang M, Zeppenfeld DM, et al. Cerebral arterial pulsation drives paravascular CSF-interstitial fluid exchange in the murine brain. *J Neurosci.* 2013;33:18190–18199.
5. Hladky SB, Barrand MA. Mechanisms of fluid movement into, through and out of the brain: evaluation of the evidence. *Fluids Barriers CNS.* 2014;11:26.
6. Saunders NR, Liddelow SA, Dziegielewska KM. Barrier mechanisms in the developing brain. *Front Pharmacol.* 2012;3:46.
7. Chen L, Elias G, Yostos MP, Stimec B, Fasel J, Murphy K. Pathways of cerebrospinal fluid outflow: a deeper understanding of resorption. *Neuroradiology.* 2015;57:139–147.
8. de Leon MJ, Li Y, Okamura N, et al. Cerebrospinal fluid clearance in Alzheimer disease measured with dynamic PET. *J Nucl Med.* 2017;58:1471–1476.
9. Louveau A, Smirnov I, Keyes TJ, et al. Structural and functional features of central nervous system lymphatic vessels. *Nature.* 2015;523:337–341.
10. Peng W, Achariyar TM, Li B, et al. Suppression of glymphatic fluid transport in a mouse model of Alzheimer's disease. *Neurobiol Dis.* 2016;93:215–225.
11. Ries M, Sastre M. Mechanisms of Aβ clearance and degradation by glial cells. *Front Aging Neurosci.* 2016;8:160.
12. Magnano C, Schirda C, Weinstock-Guttman B, et al. Cine cerebrospinal fluid imaging in multiple sclerosis. *J Magn Reson Imaging.* 2012;36:825–834.
13. ElSankari S, Balédent O, van Pesch V, Sindic C, de Broqueville Q, Duprez T. Concomitant analysis of arterial, venous, and CSF flows using phase-contrast MRI: a quantitative comparison between MS patients and healthy controls. *J Cereb Blood Flow Metab.* 2013;33:1314–1321.
14. Wolburg-Buchholz K, Mack AF, Steiner E, Pfeiffer F, Engelhardt B, Wolburg H. Loss of astrocyte polarity marks blood-brain barrier impairment during experimental autoimmune encephalomyelitis. *Acta Neuropathol (Berl).* 2009;118:219–233.
15. Klunk WE, Engler H, Nordberg A, et al. Imaging brain amyloid in Alzheimer's disease with Pittsburgh compound-B. *Ann Neurol.* 2004;55:306–319.
16. Bodini B, Veronese M, García-Lorenzo D, et al. Dynamic imaging of individual remyelination profiles in multiple sclerosis. *Ann Neurol.* 2016;79:726–738.
17. Edison P, Archer HA, Hinz R, et al. Amyloid, hypometabolism, and cognition in Alzheimer disease: an ^{11}C PIB and ^{18}F FDG PET study. *Neurology.* 2007;68:501–508.
18. Okello A, Edison P, Archer HA, et al. Microglial activation and amyloid deposition in mild cognitive impairment: a PET study. *Neurology.* 2009;72:56–62.
19. Petersen RC, Doody R, Kurz A, et al. Current concepts in mild cognitive impairment. *Arch Neurol.* 2001;58:1985–1992.
20. Polman CH, Reingold SC, Edan G, et al. Diagnostic criteria for multiple sclerosis: 2005 revisions to the "McDonald criteria." *Ann Neurol.* 2005;58:840–846.
21. Folstein MF, Folstein SE, McHugh PR. "Mini-mental state": a practical method for grading the cognitive state of patients for the clinician. *J Psychiatr Res.* 1975;12:189–198.
22. Rosen WG, Mohs RC, Davis KL. A new rating scale for Alzheimer's disease. *Am J Psychiatry.* 1984;141:1356–1364.
23. Becker JT, Boller F, Saxton J, McGonigle-Gibson KL. Normal rates of forgetting of verbal and non-verbal material in Alzheimer's disease. *Cortex.* 1987;23:59–72.
24. Wechsler D. A standardized memory scale for clinical use. *J Psychology.* 1945;19:87–95.
25. Reitan RM. Validity of the trail making test as an indicator of organic brain damage. *Percept Mot Skills.* 1958;8:271–276.
26. Freedman M, Kaplan E. Clock Drawing: A Neuropsychological Analysis. New York, NY: Oxford University Press; 1994.
27. Saxton J, Ratcliff G, Munro CA, et al. Normative data on the Boston Naming Test and two equivalent 30-item short forms. *Clin Neuropsychol.* 2000;14:526–534.
28. Benton AL. Differential behavioral effects in frontal lobe disease. *Neuropsychologia.* 1968;6:53–60.
29. Kurtzke JF. Rating neurologic impairment in multiple sclerosis: an expanded disability status scale (EDSS). *Neurology.* 1983;33:1444–1452.
30. Roxburgh RHSR, Seaman SR, Masterman T, et al. Multiple sclerosis severity score: using disability and disease duration to rate disease severity. *Neurology.* 2005;64:1144–1151.
31. Alessio AM, Stearns CW, Tong S, et al. Application and evaluation of a measured spatially variant system model for PET image reconstruction. *IEEE Trans Med Imaging.* 2010;29:938–949.

32. Veronese M, Bodini B, García-Lorenzo D, et al. Quantification of [^{11}C]PIB PET for imaging myelin in the human brain: a test-retest reproducibility study in high-resolution research tomography. *J Cereb Blood Flow Metab.* 2015;35:1771–1782.

33. Gunn RN, Coello C, Searle GE. Molecular imaging and kinetic analysis toolbox (MIAKAT): a quantitative software package for the analysis of PET neuroimaging data [abstract]. *J Nucl Med.* 2016;57(suppl):1928.

34. Jenkinson M, Beckmann CF, Behrens TEJ, Woolrich MW, Smith SM. FSL. *Neuroimage.* 2012;62:782–790.

35. Mazziotta JC, Toga AW, Evans A, Fox P, Lancaster J. A probabilistic atlas of the human brain: theory and rationale for its development. *Neuroimage.* 1995;2:89–101.

36. Montgomery AJ, Thielemans K, Mehta MA, Turkheimer F, Mustafovic S, Grasby PM. Correction of head movement on PET studies: comparison of methods. *J Nucl Med.* 2006;47:1936–1944.

37. Yushkevich PA, Piven J, Hazlett HC, et al. User-guided 3D active contour segmentation of anatomical structures: significantly improved efficiency and reliability. *Neuroimage.* 2006;31:1116–1128.

38. Acabchuk RL, Sun Y, Wolferz R, et al. 3D modeling of the lateral ventricles and histological characterization of periventricular tissue in humans and mouse. *J Vis Exp.* 2015;(99):e52328.

39. Devanand DP, Mikhno A, Pelton GH, et al. Pittsburgh compound B (^{11}C-PIB) and fluorodeoxyglucose (^{18}F-FDG) PET in patients with Alzheimer's disease, mild cognitive impairment, and healthy controls. *J Geriatr Psychiatry Neurol.* 2010;23:185–198.

40. Barrett PHR, Bell BM, Cobelli C, et al. SAAM II: simulation, analysis, and modeling software for tracer and pharmacokinetic studies. *Metabolism.* 1998;47:484–492.

41. Lindsay J, Laurin D, Verreault R, et al. Risk factors for Alzheimer's disease: a prospective analysis from the Canadian Study of Health and Aging. *Am J Epidemiol.* 2002;156:445–453.

42. Rodrigue KM, Kennedy KM, Devous MD, et al. β-amyloid burden in healthy aging: regional distribution and cognitive consequences. *Neurology.* 2012;78:387–395.

43. Bezprozvanny I, Mattson MP. Neuronal calcium mishandling and the pathogenesis of Alzheimer's disease. *Trends Neurosci.* 2008;31:454–463.

44. Mawuenyega KG, Sigurdson W, Ovod V, et al. Decreased clearance of CNS amyloid-β in Alzheimer's disease. *Science.* 2010;330:1774.

45. Xie L, Kang H, Xu Q, et al. Sleep drives metabolite clearance from the adult brain. *Science.* 2013;342:373–377.

46. Brzecka A, Leszek J, Ashraf GM, et al. Sleep disorders associated with Alzheimer's disease: a perspective. *Front Neurosci.* 2018;12:330.

47. Brass SD, Duquette P, Proulx-Therrien J, Auerbach S. Sleep disorders in patients with multiple sclerosis. *Sleep Med Rev.* 2010;14:121–129.

48. Cirrito JR, Yamada KA, Finn MB, et al. Synaptic activity regulates interstitial fluid amyloid-β levels in vivo. *Neuron.* 2005;48:913–922.

49. He XF, Liu D, Zhang Q, et al. Voluntary exercise promotes glymphatic clearance of amyloid beta and reduces the activation of astrocytes and microglia in aged mice. *Front Mol Neurosci.* 2017;10:144.

50. Paillard T, Rolland Y, de Souto Barreto P. Protective effects of physical exercise in Alzheimer's disease and Parkinson's disease: a narrative review. *J Clin Neurol.* 2015;11:212–219.

51. Kredlow MA, Capozzoli MC, Hearon BA, Calkins AW, Otto MW. The effects of physical activity on sleep: a meta-analytic review. *J Behav Med.* 2015;38:427–449.

52. Nascimento CMC, Ayan C, Cancela JM, Gobbi LTB, Gobbi S, Stella F. Effect of a multimodal exercise program on sleep disturbances and instrumental activities of daily living performance on Parkinson's and Alzheimer's disease patients. *Geriatr Gerontol Int.* 2014;14:259–266.

53. Aburub A, Khalil H, Al-Sharman A, Alomari M, Khabour O. The association between physical activity and sleep characteristics in people with multiple sclerosis. *Mult Scler Relat Disord.* 2017;12:29–33.

54. Ju YES, McLeland JS, Toedebusch CD, et al. Sleep quality and preclinical Alzheimer disease. *JAMA Neurol.* 2013;70:587–593.

55. Serot J-M, Béné M-C, Foliguet B, Faure GC. Morphological alterations of the choroid plexus in late-onset Alzheimer's disease. *Acta Neuropathol (Berl).* 2000;99:105–108.

56. Spector R, Keep RF, Robert Snodgrass S, Smith QR, Johanson CE. A balanced view of choroid plexus structure and function: focus on adult humans. *Exp Neurol.* 2015;267:78–86.

57. Ferrante F, Amenta F. Enzyme histochemistry of the choroid plexus in old rats. *Mech Ageing Dev.* 1987;41:65–72.

58. Capilla-Gonzalez V, Cebrain-Silla A, Guerrero-Cazares H, Garcia-Verdugo JM, Quiñones-Hinojosa A. Age-related changes in astrocytic and ependymal cells of the subventricular zone. *Glia.* 2014;62:790–803.

59. Sawamoto K, Wichterle H, Gonzalez-Perez O, et al. New neurons follow the flow of cerebrospinal fluid in the adult brain. *Science.* 2006;311:629–632.

60. Lisanti CJ, Asbach P, Bradley WG. The ependymal "dot-dash" sign: an MR imaging finding of early multiple sclerosis. *AJNR Am J Neuroradiol.* 2005;26:2033–2036.

61. Vercellino M, Votta B, Condello C, et al. Involvement of the choroid plexus in multiple sclerosis autoimmune inflammation: a neuropathological study. *J Neuroimmunol.* 2008;199:133–141.

62. Kivisäkk P, Mahad DJ, Callahan MK, et al. Human cerebrospinal fluid central memory CD4+ T cells: evidence for trafficking through choroid plexus and meninges via P-selectin. *Proc Natl Acad Sci USA.* 2003;100:8389–8394.

63. Reboldi A, Coisne C, Baumjohann D, et al. C-C chemokine receptor 6-regulated entry of TH-17 cells into the CNS through the choroid plexus is required for the initiation of EAE. *Nat Immunol.* 2009;10:514–523.